

Article

Synthesis of Ti Powder from the Reduction of TiCl_4 with Metal Hydrides in the H_2 Atmosphere: Thermodynamic and Techno-Economic Analyses

Mohammad Rezaei Ardani ¹, Sheikh Abdul Rezan Sheikh Abdul Hamid ^{1,*} , Dominic C. Y. Foo ^{2,*}  and Abdul Rahman Mohamed ³

¹ School of Materials and Mineral Resources Engineering, Universiti Sains Malaysia, Nibong Tebal 14300, Penang, Malaysia; mohammad.ardani@usm.my

² Department of Chemical and Environmental Engineering, Centre of Excellence for Green Technologies, University of Nottingham Malaysia, Semenyih 43500, Selangor, Malaysia

³ School of Chemical Engineering, Universiti Sains Malaysia, Nibong Tebal 14300, Penang, Malaysia; chrahman@usm.my

* Correspondence: srsheikh@usm.my (S.A.R.S.A.H.); Dominic.Foo@nottingham.edu.my (D.C.Y.F.)

Abstract: Titanium hydride (TiH_2) is one of the basic materials for titanium (Ti) powder metallurgy. A novel method was proposed to produce TiH_2 from the reduction of titanium tetrachloride (TiCl_4) with magnesium hydride (MgH_2) in the hydrogen (H_2) atmosphere. The primary approach of this process is to produce TiH_2 at a low-temperature range through an efficient and energy-saving process for further titanium powder production. In this study, the thermodynamic assessment and technoeconomic analysis of the process were investigated. The results show that the formation of TiH_2 is feasible at low temperatures, and the molar ratio between TiCl_4 and metal hydride as a reductant material has a critical role in its formation. Moreover, it was found that the yield of TiH_2 is slightly higher when CaH_2 is used as a reductant agent. The calculated equilibrium composition diagrams show that when the molar ratio between TiCl_4 and metal hydrides is greater than the stoichiometric amount, the TiCl_3 phase also forms. With a further increase in this ratio to greater than 4, no TiH_2 was formed, and TiCl_3 was the dominant product. Furthermore, the technoeconomic study revealed that the highest return on investment was achieved for the production scale of 5 t/batch of Ti powder production, with a payback time of 2.54 years. The analysis shows that the application of metal hydrides for TiH_2 production from TiCl_4 is technically feasible and economically viable.

Keywords: titanium hydride; process simulation; stability diagram; pilot production; equilibrium composition diagrams; economic evaluation



Citation: Rezaei Ardani, M.; Sheikh Abdul Hamid, S.A.R.; Foo, D.C.Y.; Mohamed, A.R. Synthesis of Ti Powder from the Reduction of TiCl_4 with Metal Hydrides in the H_2 Atmosphere: Thermodynamic and Techno-Economic Analyses. *Processes* **2021**, *9*, 1567. <https://doi.org/10.3390/pr9091567>

Academic Editor: Lukáš Richtera

Received: 30 June 2021

Accepted: 25 August 2021

Published: 1 September 2021

Publisher's Note: MDPI stays neutral with regard to jurisdictional claims in published maps and institutional affiliations.



Copyright: © 2021 by the authors. Licensee MDPI, Basel, Switzerland. This article is an open access article distributed under the terms and conditions of the Creative Commons Attribution (CC BY) license (<https://creativecommons.org/licenses/by/4.0/>).

1. Introduction

In the past decade, the rapid growth in aerospace, power generation, and biomedical industries has resulted in significant attention on the industry of titanium (Ti) and its alloys. Titanium can be used in severe conditions such as high temperature and pressure and a corrosive environment. Moreover, it has high specific strength, toughness, and biocompatibility in the human body, making it a unique choice for medical implants [1,2]. Unfortunately, the growth in the application of titanium and its alloys (compared to similar metals such as aluminum and high-alloy steels) has been affected by its production costs [3,4].

Since the invention of the Kroll process for the production of titanium, it has been the primary practical production method in the industry [5]. However, this method has several drawbacks, such as long production time, elevated production temperature, and significant energy consumption [6]. Another major obstacle in producing low-cost titanium products is that the Kroll process final output is titanium sponge. It was reported that the total cost

of traditional titanium components includes about 38% for the Ti sponge production via the traditional Kroll process, 15% related to Ti sponge refining, and the remaining 47% for the machining step, which produced almost 75% of the Ti sponge scrap [7]. Therefore, it was suggested to use powder metallurgy techniques such as additive manufacturing to produce near-net-shape products. For this purpose, the Ti sponge should be converted to Ti powder through other methods such as the hydride-dehydride (HDH) process, which is also an expensive process for the production of titanium powder [8,9].

For the mentioned reasons, many studies were conducted to introduce new techniques for Ti powder production. The two main precursors for Ti production are TiCl_4 and TiO_2 . It is noteworthy that TiCl_4 can be synthesized through the carbochlorination of TiO_2 , which is a fundamental concept of the TiRO method to produce Ti metal [10], or the ADMA process to synthesize TiH_2 powder [9]. Other potential methods are the Fray–Farthing–Chen Cambridge [11], Armstrong [12], Council for Scientific and Industrial Research Ti process [13], direct reduction of titanium slag process [14], and hydrogen-assisted magnesiothermic reduction (HAMR) [15]. Moreover, a molten salt method using TiS_2 and TiO_2 via the Ono and Suzuki process led the way to cheaper Ti metal powder production [16–18]. It was reported that the recently reported HAMR process could reduce energy consumption to about 62% of the Kroll process [11]. It should be noted that Ti has a high chemical affinity with oxygen, and it is more difficult to remove the oxygen from TiO_2 compared to reducing chlorine from TiCl_4 . Furthermore, during the reduction of TiO_2 to Ti, the synthesized byproducts of oxides are challenging to remove due to their high melting point. On the other hand, the chloride species formed as byproducts during the reduction of TiCl_4 can be easily removed. Therefore, TiCl_4 is more favorable as a precursor for continuous production.

One of the primary mineral sources for the production of Ti is ilmenite, which is a titanium-iron oxide with the main chemical phase of FeTiO_3 . Ilmenite minerals represent the most available Ti resources, with about 90% of world consumption of Ti mineral [19]. It was reported that the earth's resources of ilmenite, rutile, and anatase are more than 2 billion tons. Traditionally, ilmenite is used to produce upgraded TiO_2 [19]. However, previous studies [20,21] have shown that high-quality $\text{TiO}_x\text{C}_y\text{N}_z$ could be produced from ilmenite through low-temperature chlorination. In this method, FeTiO_3 is reduced to $\text{TiO}_x\text{C}_y\text{N}_z$ under a mixture of H_2 – N_2 gas and is subsequently purified via aeration leaching (Becher process) with ammonium chloride (NH_4Cl) lixiviant to remove metallic iron. The obtained $\text{TiO}_x\text{C}_y\text{N}_z$ is then chlorinated at 400 °C to produce TiCl_4 gas [22,23]. The author proposed directly reacting the obtained TiCl_4 gas with metal hydrides such as MgH_2 to produce TiH_2 powder at low-temperature ranges under the hydrogen (H_2) atmosphere [24–26]. The TiH_2 powder can then transform into Ti powder through the dehydrogenation process in a vacuum. The primary benefit of producing TiH_2 as an intermediate component is that the Ti powder can be produced with shallow oxygen content [27]. This phase is insoluble in water and diluted acid, which allows it to be separated from other products via acid leaching [28].

The feasibility of the proposed method was analyzed through chemical reactions involved in the production method and the obtained economic parameter. Technoeconomic analysis was also carried out using the SuperPro Designer software. The purpose of such analysis is to identify a production scale that has attractive economic performance. It is an important step in process development and commercialization. Data of laboratory-scale experimental may be used to perform process simulation study prior to pilot-scale testing. In the process industry, various technoeconomic works have been reported with the use of process simulation tools. For instance, Granjo et al. [29] made use of Aspen Plus and Monte Carlo simulation to evaluate different manufacturing methods of sodium methoxide. More recent works on technoeconomic analysis based on Aspen Plus simulation have been reported for supercritical CO_2 extraction of *Eucalyptus globulus* bark [30], chitin nanomaterials production [31], and anaerobic digestion of sugarcane vinasses for biogas production [32]. Moreover, there were authors who reported the use of SuperPro Designer

for technoeconomic analysis of various biochemical, pharmaceutical, and food processes. Some of the early works were reported by Petrides and coworkers [33] for pharmaceutical processes. Later works on SuperPro Designer were reported for debottlenecking studies, for pharmaceuticals [34,35], and for fine chemicals [36]. More recently, SuperPro Designer was used for technoeconomic analysis for various manufacturing processes of chemicals, biochemicals, and food. These include the production of cocoa butter [37], monoclonal antibody [38], biodiesel [39], nanomaterials [40], catechin [41], biomass pyrolysis products [42], and thorium extraction from monazite [43]. It is also worth noting that Monte Carlo simulations were also reported for use in some of the above works where SuperPro Designer was utilized (e.g., [38,40]). This allows for the identification of important parameters that affect the economic characteristics of the process.

The current study attempts to address the thermodynamic, operational, and economic evaluation of the TiCl_4 reduction process with MgH_2 under H_2 atmosphere for the production of TiH_2 , which could be further dehydrogenated to Ti powder. The thermodynamic assessment was used to study the effect of temperature, partial pressure, and the molar ratio of the TiCl_4 to reductant on the formation efficiency of TiH_2 . Economic analysis was investigated for several production scales in order to identify critical economic parameters such as production revenue and gross margin. Moreover, sensitivity analyses were performed to evaluate the effect of different operating parameters on the economic performances of the selected production scale.

2. Materials and Methods

The processing cycle in the present study, developed for the production of Ti powder from ilmenite, is shown in Figure 1. In the first step, the ilmenite is reduced under $\text{H}_2\text{-N}_2$ atmosphere to convert iron oxides present in the ilmenite to metallic iron. In the subsequent step, metallic iron is separated from the nitrated ilmenite through aeration leaching (Becher process). Following the filtration process, the leftover powder is $\text{TiO}_x\text{C}_y\text{N}_z$ which can be employed in the chlorination process. The product of the chlorination process is TiCl_4 gas. The complete explanation of the reduction and chlorination process of ilmenite is discussed elsewhere [20–22]. The produced TiCl_4 liquid is converted to gas above $150\text{ }^\circ\text{C}$ and reacted with MgH_2 to synthesize TiH_2 powder via Equation (1). The TiH_2 can be separated from reaction byproducts through acid leaching and washing with distilled water to remove the MgCl_2 . Next, the filtered TiH_2 powder is dried for 12 h in an oven, and it can be converted to Ti powder via heating under Ar gas for dehydrogenation. Details of the latter process are listed elsewhere [44,45].

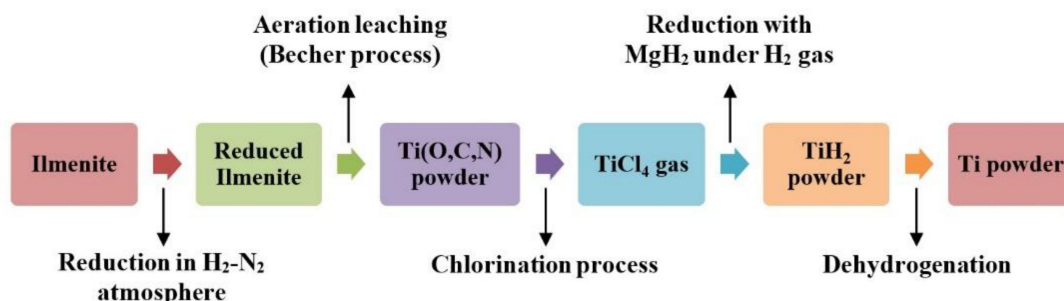


Figure 1. Schematics of a proposed process of Ti powder production from ilmenite.

2.1. Thermodynamic Calculation

Previous studies [46,47] have discussed the thermodynamic principles of iron removal from nitride ilmenite. This study investigated the thermodynamic equilibrium of TiH_2 synthesis from TiCl_4 using MgH_2 as a reductant. This calculation was helpful for studying

the possible species formation during the reaction. The HSC Chemistry v6.0.0 software (Outokumpu Research Oy, Tornio, Finland) was used for thermodynamic analysis and calculations. Thermochemical calculations are valuable tools for developing new chemical processes and mechanisms. This software provides powerful calculation methods to investigate different variables' effects on the chemical system at equilibrium [48].

2.2. Synthesis Process

In previous studies [21,22], the preparation of TiCl_4 gas from ilmenite was elaborated. In the current study, the TiH_2 was synthesized from TiCl_4 gas reacted with the MgH_2 powder at 500 °C for 12 h at the lab scale. Our previous attempts to synthesize TiH_2 at a temperature between 250 and 500 °C indicated that higher temperatures positively impacted the formation of TiH_2 [24–28]. The reduction products were then washed with water and diluted HCl to separate TiH_2 powder from the reaction byproducts. The X-ray diffraction (XRD) technique was employed for the study of phase evolution after the reduction process using Cu-K α radiation ($\lambda = 1.5404 \text{ \AA}$, Bruker D8-advance, Billerica, MA, USA). The morphology and surface elemental analysis of the powder in each experimental step was studied with a field emission scanning electron microscopy equipped with electron dispersive X-ray spectroscopy (FESEM/EDX, Leo Supra 35VP, Oberkochen, Baden-Württemberg, Germany).

2.3. Economic Evaluation

In order to investigate the commercialization potential of the proposed method for the production of Ti metal powder, the technoeconomic assessment (TEA) was conducted using the SuperPro Designer software v8.5 [49]. The TEA calculates the production expenses, technology, and scaling-up issues of the product. The effect of individual economic parameters, i.e., costs of raw material, equipment costs, and energy consumption, on the capital cost investment of a pilot plant was evaluated. The economic performance was investigated for the three production scales, i.e., 1000 kg (1 t/batch), 5000 kg (5 t/batch), and 10,000 kg (10 t/batch) per batch of the final product (Ti powder).

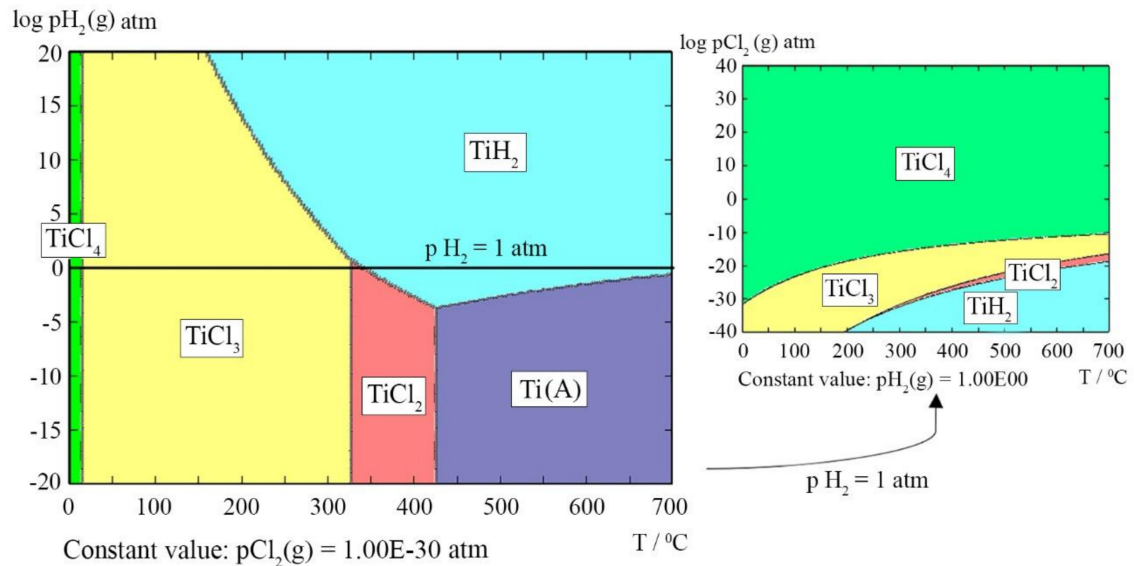
3. Results

3.1. Thermodynamic Assessment

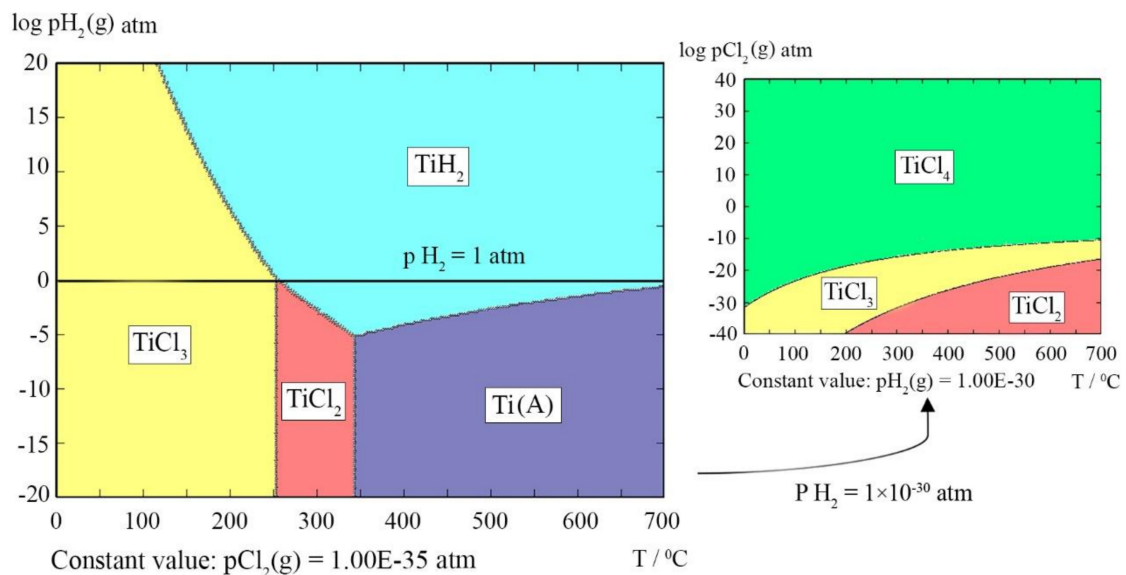
The standard change in Gibbs free energy of formation (ΔG_f°) of the chemical species that were used in this study is listed in Table 1. The thermodynamic data were extracted from Stull and Prophet (1971) [50] for the temperature range of 0–700 °C, except for MgH_2 , which was extracted from Brain (1997) [51] for the thermodynamic data up to 700 °C. The thermodynamics study on converting ilmenite to nitride ilmenite and subsequently TiCl_4 was published elsewhere [52,53]. The chemical potential diagrams (stability diagrams) of the M-Cl-H (M: Ti and Mg) systems at different partial pressures in Table 1 are illustrated in Figures 2 and 3. The phase stability diagrams demonstrated the stability boundaries of each phase in a ternary system as a function of temperature or in isothermal conditions. The stability diagrams were calculated based on the Gibbs free energy minimization. The partial pressure of gas species was calculated from the equilibrium constant and the activity of the gas species.

In Figures 2 and 3, the effect of temperature, the partial pressure of H_2 (P_{H_2}), and partial pressure of chlorine (P_{Cl_2}) on the stability of associated phases are illustrated. Figure 2 illustrates the Ti-Cl-H diagrams with the change in the partial pressure of H_2 gas. The values of the P_{Cl_2} were changed, starting from 1 atm until the appearance of TiH_2 phase at $P_{\text{H}_2} = 1 \text{ atm}$ below 500 °C. It was observed that for $P_{\text{Cl}_2} \leq 1 \times 10^{-30} \text{ atm}$, the TiH_2 phase was stable within the specified temperature range. It can be seen from Figure 2a that in the Ti-Cl-H system, the dominant solid phase at $T \leq 350 \text{ °C}$ and $P_{\text{H}_2} = 1 \text{ atm}$ was TiCl_3 , and at the higher temperature range, the TiH_2 phase was more stable. Moreover, Figure 2b shows that with additional decreasing in the P_{Cl_2} to 10^{-35} atm , there was no presence of TiCl_4 , and the TiH_2 stability area increased to $T \geq 250 \text{ °C}$. According to Figure 2a, the equilibrium

interface between TiH_2 and TiCl_3 indicated that the stability area of TiH_2 started at a temperature above about 150°C and $P_{\text{H}_2} = 20$ atm, and with an increase in temperature, it was expanded to P_{H_2} of 1 atm at a temperature around 300°C . This particular distinction between the two diagrams in Figure 2a,b represents the importance of the effect of P_{H_2} and P_{Cl_2} on the stability diagrams. Hence, in the presence of H_2 atmosphere, it should be possible to reduce the TiCl_4 to TiH_2 .



(a)



(b)

Figure 2. Ti-Cl-H predominance diagram at a partial pressure of Cl_2 (a) $P_{\text{Cl}_2} = 1 \times 10^{-30}$ atm; (b) $P_{\text{Cl}_2} = 1 \times 10^{-35}$ atm.

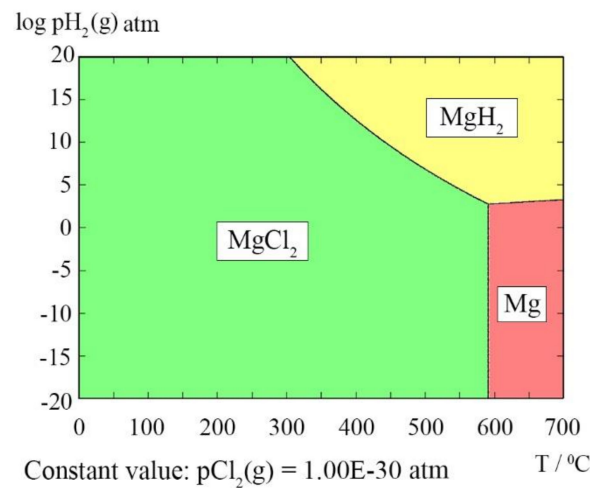


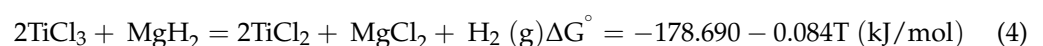
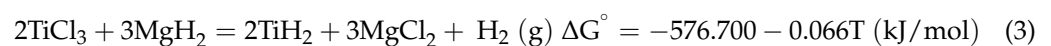
Figure 3. Mg-Cl-H predominance diagram at $P_{Cl_2} = 1 \times 10^{-30}$ atm.

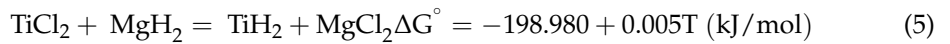
Table 1. Standard Gibbs free energy of formation for the compounds in the investigated system from 0 to 700 °C.

Component	Standard Gibbs Energy of Formation (ΔG_f°) (kJ/mol)	Reference
HCl (g)	$\Delta G_f^\circ = -93.084 - 0.008T$	[50]
MgCl ₂	$\Delta G_f^\circ = -638.230 + 0.157T$	[50]
MgH ₂	$\Delta G_f^\circ = -78.504 + 0.139T$	[51]
TiCl ₂	$\Delta G_f^\circ = -512.330 + 0.158T$	[50]
TiCl ₂ (g)	$\Delta G_f^\circ = -238.000 - 0.022T$	[50]
TiCl ₃	$\Delta G_f^\circ = -716.800 + 0.212T$	[50]
TiCl ₃ (g)	$\Delta G_f^\circ = -539.510 + 0.049T$	[50]
TiCl ₄ (g)	$\Delta G_f^\circ = -762.400 + 0.119T$	[50]
TiH ₂	$\Delta G_f^\circ = -147.290 + 0.140T$	[50]
Ti ₂ Cl ₆ (g)	$\Delta G_f^\circ = -245.430 - 0.018T$	[51]

In order to further highlight the effect of P_{H_2} on the phase stability, the Ti-Cl-H predominance diagram was plotted for a constant amount of P_{H_2} at 1 atm in Figure 2a and 1×10^{-30} atm in Figure 2b. As is illustrated in Figure 2a to obtain the TiH₂ predominance area at $P_{H_2} = 1$ atm, the P_{Cl_2} in the system must be as low as 1×10^{-30} atm for $T = 350$ °C and 1×10^{-35} atm for $T = 250$ °C. However, it can be observed from Figure 2b that at constant P_{H_2} of 1×10^{-30} atm, there was no presence of TiH₂. This is the main reason that there was a need to run the reduction process in the presence of H₂ gas instead of an inert atmosphere. Basically, in $P_{H_2} \geq 1$ atm and very low amount of P_{Cl_2} , TiH₂ was a predominant phase. Previous work by Udayakumar et al. [54,55] in producing TiH₂ in an inert atmosphere showed a low yield and validating this thermodynamics analysis.

It should be emphasized that depending on the partial pressure of Cl₂, the system may enter the predominance area of TiCl₃ and possibly TiCl₂. This particular scenario indicates a possible thermochemical mechanism that TiH₂ may produce from reactions between TiCl₃ or TiCl₂ and MgH₂ rather than the reaction via Equation (1) at a fixed temperature and certain P_{H_2} and P_{Cl_2} . In this regard, the possible reactions in the system could be followed as in Equations (2)–(5) for the TiCl₄-MgH₂ reaction system.





The predominance diagram for the Mg-Cl-H system at $P_{\text{Cl}_2} = 1 \times 10^{-30}$ atm is shown in Figure 3. The interface between MgH_2 and MgCl_2 indicated the stability of metal chlorides at $P_{\text{H}_2} = 1$ atm and almost the whole temperature range, except for Mg, which is more stable at a temperature above 600 °C, according to Figure 3. From the latter figure, MgH_2 was a stable phase at a temperature above 350 °C and higher P_{H_2} . As a result, it is possible to conclude that reducing TiCl_4 with metal hydrides is possible, and the stable phases were TiH_2 and MgCl_2 , depending on the partial pressure of chlorine gas. On a side note, this thermodynamics approach does not consider the possibility of simultaneous formation of different species in the same system, as only one species, for example, TiCl_3 or TiH_2 , is described as a feasible component at a particular condition. Given this, the Gibbs free-energy minimization method was carried out to evaluate the formation of various phases simultaneously.

Phase Composition Diagrams

The objective of this section is to present the equilibrium composition diagrams as in Table 1. Therefore, calculations were carried out for stoichiometric and nonstoichiometric amounts of reactants for the temperature range of 0–700 °C as given in Equation (1). The phase determination of the system at equilibrium condition was calculated with the help of the equilibrium module of HSC Chemistry v6.0.0 (Tampere, Southern Finland, Finland), which is based on the minimization of the Gibbs free energy [56]. The relevant elements (Ti, Cl, Mg, and H) with an ideal behavior were used to determine the stable phases of the system under the investigated conditions. It should be noted that a constant amount of H_2 equaling 2 mol was considered in all the calculations for the effect of excess H_2 in the system since the reduction experiment suggested proceeding under H_2 atmosphere. The molar ratio of TiCl_4 : MgH_2 was 1:2 for stoichiometric conditions according to Equation (1). In this condition, the final equilibrium phases after reactions were TiH_2 , MgCl_2 , and H_2 in all temperature range according to Equation (1).

Furthermore, the nonstoichiometric conditions with increasing the molar ratio of TiCl_4 : MgH_2 in Equation (1) were investigated with an increase in the latter molar ratio to 2:2 and 3:2, as shown in Figure 4. The changes in the molar ratio of the reactants affected the final products available in the reaction. From Figure 4, TiH_2 was formed at its highest amount of 0.6 mol below 100 °C. As the temperature raised to 700 °C, the TiH_2 molar amount gradually dropped to 0.1 mol when the TiCl_4 molar amount increased to 2 mol, as shown in Figure 4a. However, Figure 4b illustrates that with an additional increase in TiCl_4 to 3 mol, TiH_2 was not present above 100 °C.

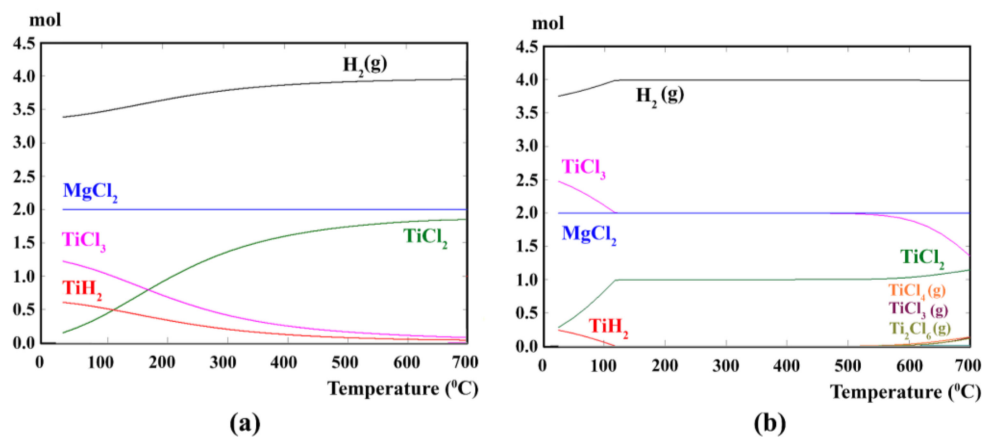
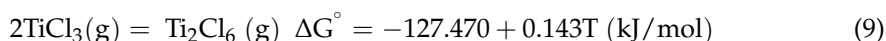
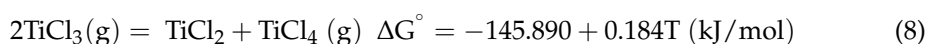
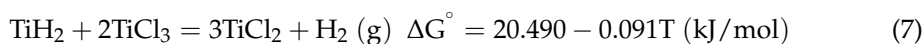


Figure 4. Theoretical equilibrium phase composition calculated for molar ratio of (a) TiCl_4 : $\text{MgH}_2 = 2:2$ and (b) TiCl_4 : $\text{MgH}_2 = 3:2$.

Furthermore, by increasing the $\text{TiCl}_4\text{:MgH}_2$ molar ratio to 3:2, the TiCl_3 phase formed, in addition to TiH_2 . At a TiCl_4 amount of 2 mol, TiCl_3 decreased continuously from about 1.2 to 0.1 mol, with temperatures shown in Figure 4a. However, by increasing the $\text{TiCl}_4\text{:MgH}_2$ molar ratio to 3:2, the change in the TiCl_3 amount was different, as shown in Figure 4b. It can be observed that the TiCl_3 amount dropped to about 2 mol at 100 °C, and there was no change up to 500 °C. Then, there was another decrease in the TiCl_3 amount from 2 to 1.3 mol above 550 °C. In addition, the amount of MgCl_2 as a final product in the system was constant in all the diagrams. According to Figure 4, it was clear that with increasing temperature, the molar amount of H_2 gas gradually increased up to about 4 mol at a TiCl_4 molar amount of 2 mol. It was also rapidly increased to about 4 mol when the TiCl_4 molar amount was 3 mol, and it was constant above 150 °C. Moreover, it shows the formation of H_2 gas in the system with an increase in a molar ratio of $\text{TiCl}_4\text{:MgH}_2$.

Another essential feature of diagrams in Figure 4 is the formation of the TiCl_2 phase as a product with the reverse chemical behavior of TiCl_3 and TiH_2 . While the molar amount of TiCl_3 and TiH_2 decreased, the molar amount of TiCl_2 began to increase. Since TiH_2 , TiCl_3 , and TiCl_2 were behaving comparably, there should be a reaction to consuming the first two phases to convert to a later one with increasing temperature. Moreover, at TiCl_4 molar amount of 3 and temperature range above 600 °C, interesting changes occurred as new gas phases, namely TiCl_3 (g), TiCl_4 (g), and Ti_2Cl_6 (g), were formed, and the amount of TiCl_2 started to increase. The main reason for these behaviors is the possibility of the reaction between excess TiCl_4 and the produced TiH_2 in the system as Equation (6), which has negative ΔG° below 700 °C. In addition, the produced TiCl_3 can be reacted with TiH_2 to produce TiCl_2 as Equation (7). Moreover, the formation of TiCl_3 (g), TiCl_4 (g), and Ti_2Cl_6 (g) are due to the transformation of TiCl_3 to the gas phase above 500 °C. Up to 500 °C, the TiCl_3 is in the solid state, and with an increase in temperature, it is completely decomposed to the gaseous state. Subsequently, the amount of TiCl_3 decreased above 500 °C. As a result, TiCl_2 and TiCl_4 (g) can be produced according to Equation (8). In addition, there is the possibility that TiCl_3 (g) transforms to Ti_2Cl_6 (g) phase, whereas this reaction has negative ΔG° according to Equation (9).



To put it briefly, the formation of TiH_2 is possible through a reaction between MgH_2 or CaH_2 and TiCl_4 ; however, the ratio between TiCl_4 and metal hydrides was critically important to have TiH_2 following the completion of the reactions in the system.

The equilibrium molar amount and molar fraction of TiH_2 ($X_{\text{TiH}_2}^\circ$) as a function of the molar fraction of TiCl_4 ($X_{\text{TiCl}_4}^\circ$) and temperature for the $\text{TiCl}_4\text{-MgH}_2$ reaction system are provided in Figure 5. X_p° was defined as Equation (10).

$$X_p^\circ = \frac{n_i^\circ}{\sum n_p^\circ} \quad (10)$$

where n_i° is an output mole of component i in the system (i.e., TiCl_4 or TiH_2), and n_p° is the molar amount of all the products after the reduction process based on the equilibrium composition calculation data from HSC software for Equation (2)–(9). For the sake of simplification, the amount of MgH_2 was set to 2 mol, similar to previous calculations for equilibrium compositions. It was evident from Figure 5a that TiH_2 formation started at $X_{\text{TiCl}_4}^\circ = 0.1$, and its equilibrium amount increased slightly with the molar fraction of TiCl_4 to reach its maximum of 1 mol when $X_{\text{TiCl}_4}^\circ$ was almost 0.3. According to Figure 5b, for $X_{\text{TiCl}_4}^\circ$ between 0.1 and 0.3, the molar fraction of TiH_2 decreased with increasing temperature. In

general, TiH_2 can be produced when $X_{\text{TiCl}_4}^\circ$ was between 0.1 and 0.5 for all temperature range, and its equilibrium amount reaches the highest amount at $X_{\text{TiCl}_4}^\circ$ between almost 0.3 and 0.4 in all temperature range. With more TiCl_4 addition at a constant amount of MgH_2 , the formation of TiH_2 was impeded, while TiCl_3 or TiCl_2 phases began to produce, as discussed in Figure 4. Needless to say, all the calculations are based on thermodynamic data and minimization for the ΔG° in the system.

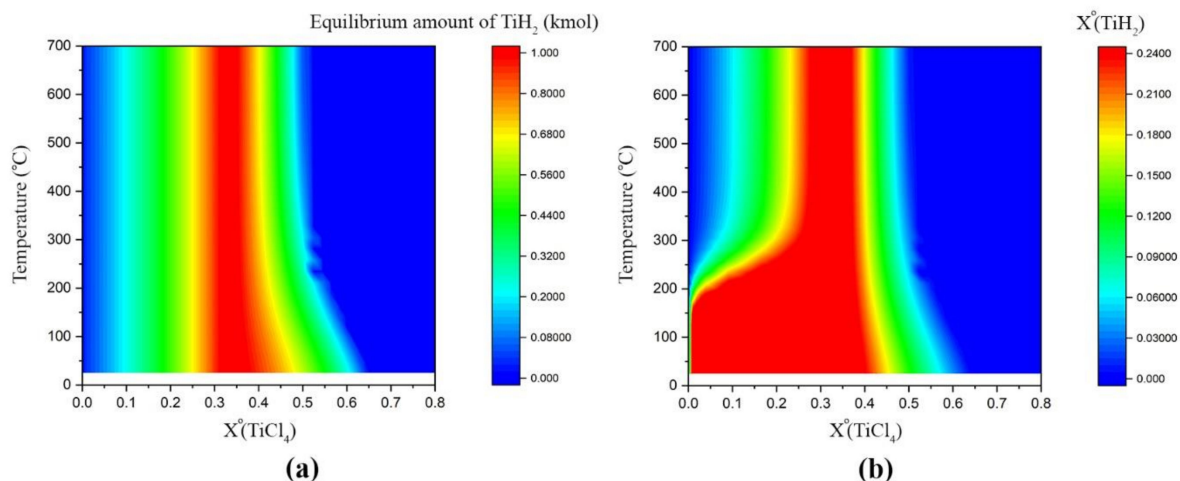


Figure 5. Effect of $X_{\text{TiCl}_4}^\circ$ in TiCl_4 - MgH_2 reaction system on (a) equilibrium amount of TiH_2 and (b) equilibrium TiH_2 mole fraction.

Since TiCl_4 can be reduced to TiH_2 , TiCl_3 , and TiCl_2 via Equations (6)–(9) solely based on the molar ratio between TiCl_4 and MgH_2 , it is of interest to know the optimum molar fraction of TiCl_4 to MgH_2 , which can reach the highest yield of TiH_2 . If TiH_2 production efficiency was defined as the molar amount of produced TiH_2 as in Equations (2)–(9) divided by the stoichiometric molar amount of TiH_2 from Equation (1), then Figure 6 could be plotted for the TiCl_4 - MgH_2 reaction system. It can be observed from Figure 6 that the TiH_2 efficiency reached the highest level of 100% for the amount of $X_{\text{TiCl}_4}^\circ$ below 0.3 for all temperature ranges. In this condition, no TiCl_3 or TiCl_2 was produced, and TiCl_4 was entirely transformed to TiH_2 . In addition, an excess amount of MgH_2 could be retained in the system. Moreover, the calculated data showed that change in the temperature had no significant effect on the TiH_2 formation efficiency, except a slight increase in TiH_2 efficiency at a temperature below 250°C and fraction between $0.4 < X_{\text{TiCl}_4}^\circ < 0.5$. It should be noted that these calculations were based on the equilibrium assumption, and the situation in the real system could be different.

3.2. Phase Analysis

The synthesis of TiH_2 was performed using MgH_2 powder as a reductant according to the process of Figure 1. The phase analysis of the final reduction products was employed to gauge the mechanism of the reaction according to Equations (1)–(9). Figure 7 represents the XRD diffraction patterns for raw ilmenite, reduced ilmenite before and after the Becher process, and the reduced powder with MgH_2 at 500°C for 12 h. The ICSD reference number of the studied phases are 98-003-5383 (FeTiO_3), 98-001-7721 (Fe_2TiO_5), 98-008-9933 ($\text{TiO}_x\text{C}_y\text{N}_z$), 98-008-7922 (Fe), 98-008-8801 (MgH_2), 98-008-9526 (Mg), 98-001-1144 (TiCl_3), 98-009-6474 ($\text{MgCl}_2 \cdot (\text{H}_2\text{O})_4$), 98-000-3817 (TiO_2), and 98-006-5530 (TiH_2). It is evident from Figure 7 that the raw ilmenite mainly consists of FeTiO_3 and pseudobrookite (Fe_2TiO_5). All the ICSD# for phases detected were listed in Figure 7. Moreover, low-intensity peaks related to titanium dioxide (TiO_2) were also observed. It is shown in Equation (11) that ilmenite can be converted to the TiN through the carbothermal reduction and nitridation (CTRN) process. Previous studies by Rezan et al. [57,58] reported that the actual phase

from the carbothermal reduction and nitridation of ilmenite was $\text{TiO}_x\text{C}_y\text{N}_z$ rather than TiN. On the other hand, the Fe_2TiO_5 phase was transformed to FeTiO_3 via the reaction of Equation (12).

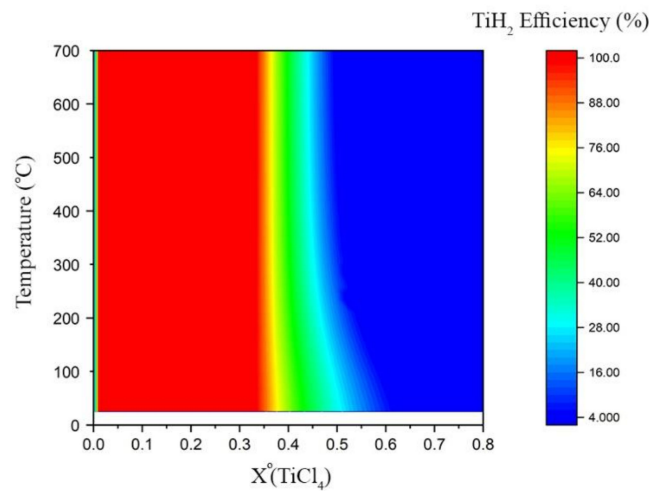
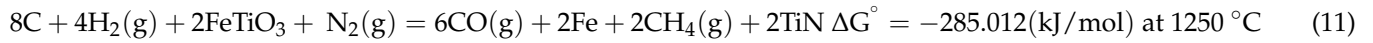


Figure 6. Effect of $X_{\text{TiCl}_4}^\circ$ on TiH_2 formation efficiency in the temperature range up to 700°C for $\text{TiCl}_4\text{-MgH}_2$ reaction system.

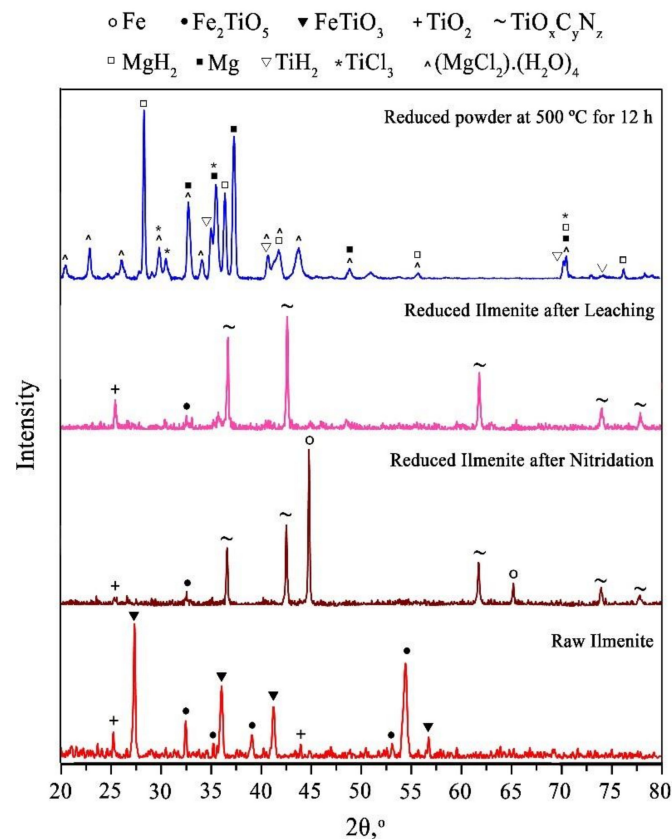


Figure 7. XRD analysis data for raw ilmenite, nitrided ilmenite before and after Becher process, and reduction process of TiCl_4 with MgH_2 at 500°C for 12 h.

Figure 7 shows that the reduced powder after nitridation was a combination of the $TiO_xC_yN_z$ phase and metallic Fe as expected from Equation (11). This powder was later leached according to the Becher process [20], and the metallic Fe was removed entirely, as can be seen from the XRD data in Figure 7. The Fe particles can react with dissolved oxygen as Equation (13) to form iron oxide hydrate ($Fe_2O_3 \cdot xH_2O$).

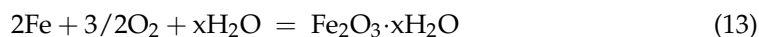


Figure 7 it can be observed that in addition to the TiH_2 phase, other phases such as $TiCl_3$, MgH_2 , and Mg were detected. Moreover, $MgCl_2(H_2O)_4$ was formed as a major byproduct of the reaction system. This phase was produced due to moisture adsorption on $MgCl_2$. The formation of $TiCl_3$ can be explained through Equation (14). It was reported that in the Ti-Cl-H system, $TiCl_4$ has a high tendency to reduce to $TiCl_3$ in the presence of H_2 gas [59]. Simultaneously, $TiCl_3$ can react with MgH_2 powder to produce TiH_2 by Equation (15). Therefore, the possible chemical pathway for the production of TiH_2 from $TiCl_4$ reaction with MgH_2 could be from Equations (14) and (15). It should be noted that the presence of Mg in the XRD data results from the partial dehydrogenation of MgH_2 powder. Overall, the XRD patterns confirmed the formation of TiH_2 from the proposed method.

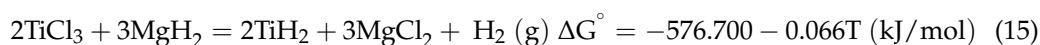


Figure 8a–c illustrate the as-received ilmenite morphology together with the reduced ilmenite before and after the leaching process. Besides this, the morphology of the TiH_2 powder after washing the reduction products with distilled water and diluted HCl is illustrated in Figure 8d. Figure 8a–c indicates the formation of spherical-shaped particles, which could be related to the formation of metallic iron, and it can be easily removed from the system through the Becher process. The EDX analysis data of Figure 8c clearly shows the high percentage of Fe content from nitrated ilmenite with a spherical Fe particle forming due to the interaction of carbon saturated molten iron. Figure 8d demonstrates the morphology of the final powder after the reaction between $TiCl_4$ gas and MgH_2 powder. It can be observed that irregularly shaped particles were formed during the reduction process. The EDX analysis data of these particles demonstrated the presence of about 78 wt% Ti with the balance oxygen. The presence of oxygen in the EDX analysis data should be the result of the oxidation of TiH_2 surface, which was previously reported by Zhang et al. (2017) [60] that an oxide layer could be formed on the TiH_2 surface. The phase analysis and morphology study of the final powders indicated the formation of the TiH_2 powder with irregularly shaped particles from the reduction of $TiCl_4$ gas with MgH_2 powder.

3.3. Process Simulation and Economics Evaluation

In the previous section, the experimental results for the production of TiH_2 powder via thermodynamic assessment (Section 3.1) and phase and morphology characterization (Section 3.2) are presented. The results show that TiH_2 powder production from the proposed method was feasible technically. However, to examine the cost-effectiveness of the process, it is beneficial to investigate the economic behavior of the production process. Thus, in this section, the TEA was performed for the production of TiH_2 powder from ilmenite and subsequently Ti metal powder from TiH_2 as a final product. It is necessary to estimate the total production costs of the product before any financial investment is made for a pilot production [61].

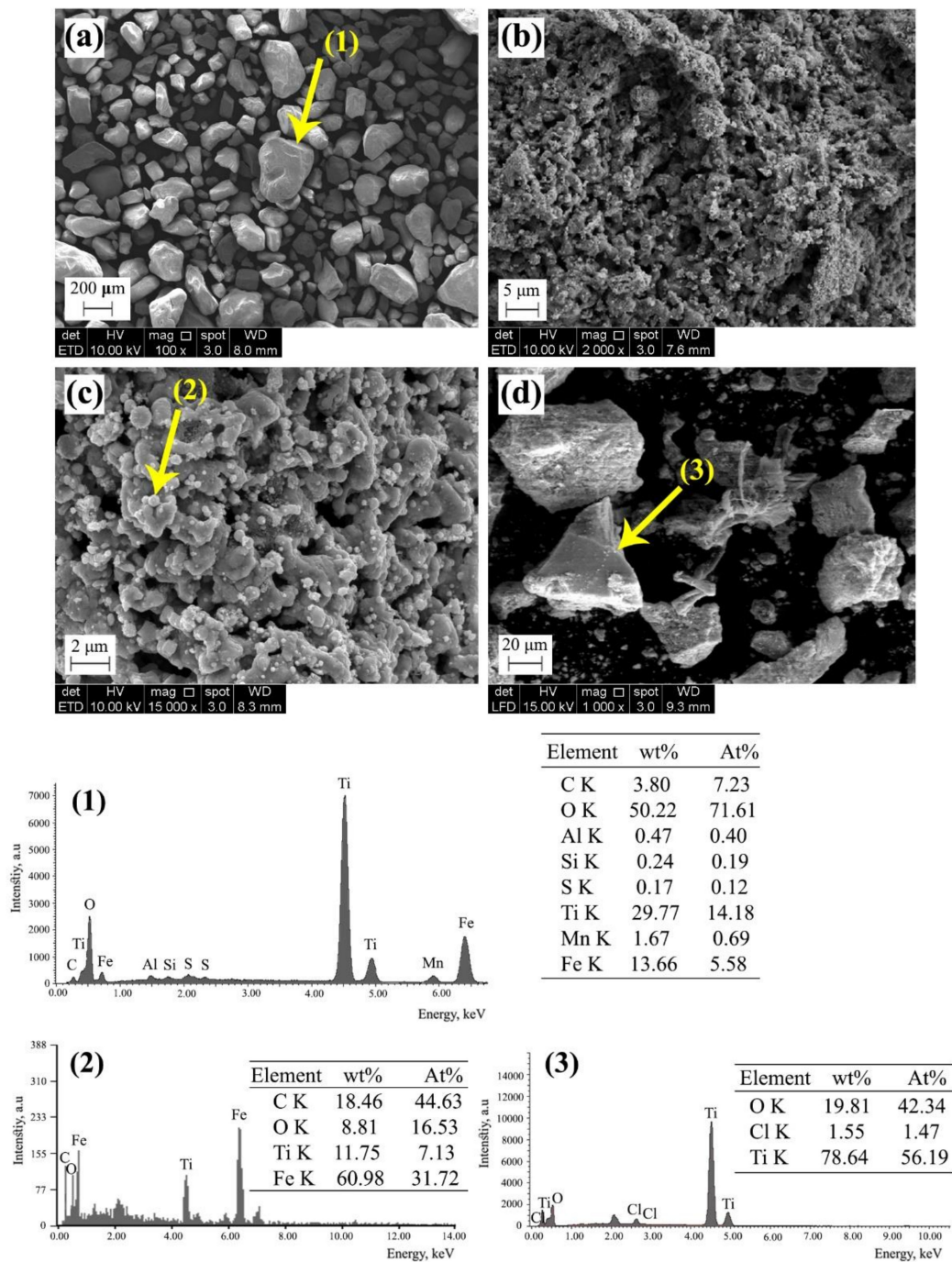


Figure 8. SEM images for: (a) as-received ilmenite, (b) reduced ilmenite under H_2-N_2 atmosphere, (c) reduced ilmenite after leaching process with spherical Fe particles, and (d) TiH_2 powder after water washing and acid leaching. (Point (1) is EDX analysis micrograph for raw ilmenite, point (2) is EDX analysis micrograph for spherical particles in reduced ilmenite, and point (3) is EDX micrograph for obtained TiH_2 powder after water washing and acid leaching).

Figure 9 shows the simulation flowsheet developed using SuperPro Designer [49] for Ti powder production from ilmenite ore. As shown, the ilmenite was grounded below $75 \mu m$ in procedure P-1 (Grinder GR-101), and it was mixed with coal in the procedure P-1/2. Next, the mixture was subjected to the CTRN process in reactor P-2 (vessel R-101) at $1250 \text{ }^\circ C$ for 5 h in the presence of H_2 and N_2 gases [62]. In the proposed method, plastic wastes such as polyethylene terephthalate (PET) can be used instead of coal since they are valuable carbon resources. It has been reported that PET stands as 8 wt% of the global solid

waste [23]. In our previous studies [22,23], it was shown that the ilmenite could be reduced with PET via the CTRN process. Compared to the conventional method for the reduction of ilmenite, this is a sustainable method for recycling waste plastics from economic and environmental aspects.

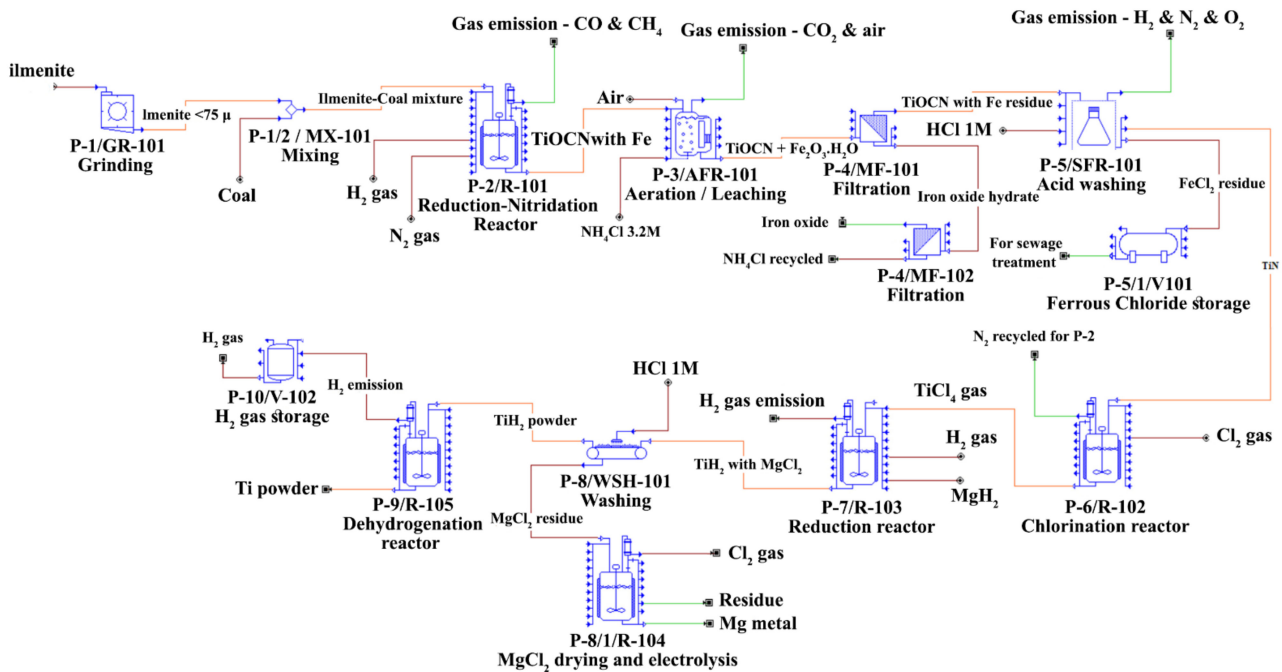
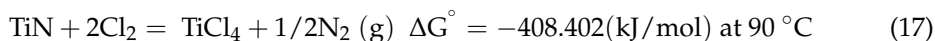


Figure 9. Simulation flowsheet for titanium powder production in SuperPro Designer.

As it was shown in Equation (11), the reduction products were the mixture of TiN and Fe particles. After completing the reduction step, Fe particles were separated from TiN through aeration leaching using the Becher process (procedure P-3) [63]. For this purpose, air and ammonium chloride (NH_4Cl 3.2 M) were injected into the leaching vessel AFR-101 for aqueous iron oxidation. The Fe particles can react with dissolved oxygen following the reaction stoichiometry in Equation (13) to form an iron oxide hydrate ($\text{Fe}_2\text{O}_3 \cdot x\text{H}_2\text{O}$). Later, the mixture was sent for filtration in the filter unit MF-101 (procedure P-4). The filtrate from the latter contains dissolved NH_4Cl and aqueous $\text{Fe}_2\text{O}_3 \cdot x\text{H}_2\text{O}$, which can be separated from each other through filtration (procedure P-4/MF-102). Although the leaching process (P-3) was performed at 90°C for 7 h to ensure complete oxidation of Fe, there is the possibility that a small portion of Fe particles remains in the TiN filter cake [63]. Therefore, the filter cake was washed with hydrochloric acid (HCl; 1 M) in procedure P-5 to remove all remaining Fe particles. The latter can be transformed into iron chloride (FeCl_2), following Equation (16). The FeCl_2 residue is collected in tank P-5/1 (vessel V101), which can be sold as a byproduct for the sewage treatment industry or recycled back to Fe_2O_3 for the ironmaking industries [64,65].

A batch vessel reactor (P-6/R-102) is used to model the chlorination of TiN powder. The chlorination process was performed at 400°C for 5 h, in the presence of Cl_2 gas, which converts TiN to TiCl_4 gas following Equation (17) [66]. It is worth noting that the product N_2 gas can be collected and reused in procedure P-2. The TiCl_4 gas can be reduced with MgH_2 to form a solid mixture of TiH_2 and MgCl_2 , following the reaction stoichiometry in Equation (1). This process was carried out in the reduction reactor P-7 (R-103), in which the MgH_2 powder was used as a reductant agent in the reduction of TiCl_4 to TiH_2 . This mixture is then subjected to water washing (P-8/WSH-101) for the removal of MgCl_2 , which is water soluble. The solution residue from water washing is then sent to the electrolysis (procedure P-8/1) for Mg metal production, which can later be reacted with H_2 gas to

produce MgH_2 for the reduction process. On the other hand, the TiH_2 powder is used as a raw material for a dehydrogenation reactor (P-9) for Ti powder production [23,24]. It should be noted that the H_2 gas emission from procedures P-7 and P-9 can be collected and stored in vessel P-10/V-102 for further application in the ilmenite reduction process (P-2).



The main benefit of the current method compared to the traditional Kroll process is that the final product is TiH_2 or Ti metal powders rather than Ti sponge. Therefore, instead of machining the Ti sponge to produce final products that generate a large amount of scrap, the TiH_2 or Ti metal powder can be directly used in powder metallurgy techniques to generate the final products with less scrap and reduce energy consumption related to the machining step, resulting in an enhanced environmental impact. Moreover, the reaction temperature in the reduction reactor P-7 (R-103) is 500°C , which is much lower than $900\text{--}950^\circ\text{C}$ in similar processes, where the TiCl_4 reduction is performed with molten Mg which requires a high temperature to melt Mg metal [9]. However, the current study proposes to employ MgH_2 powder at a lower temperature with less energy consumption, which is more environmentally friendly. Another major difference is that the reaction byproducts from reactor P-7 (R-103) separated via hydrometallurgical technique in process P-8 instead of using vacuum distillation at elevated temperature of $1000\text{--}1050^\circ\text{C}$ in similar processes [67].

The production process simulation was performed for the annual operation time of 7920 h/year, plant construction duration of 6 months and project lifetime of 15 years. The processing time and unit for the respective procedures of the model are summarized in Tables A1 and A2 in Appendix A. In addition, Table 2 summarizes the overall process parameters for different production scales. It can be observed that by increasing the production scale, the recipe batch time and recipe cycle time are increased, and the number of annual batches dropped. However, due to larger process throughput, the total amount of Ti product increases for the larger production capacity (e.g., 10 t/batch).

Table 2. Overall process parameters for process simulation for different production scales of Ti powder.

Parameter	1 t/batch	5 t/batch	10 t/batch
Utilized annual operation time (h/year)	7914.24	7898.54	7894.90
Recipe batch time (h)	60.24	83.45	124.09
Recipe cycle time (h)	14.00	31.26	61.19
Number of batches per year	562	251	128
Total amount of Ti produced (kg/year)	562,000	1,255,000	1,280,000

3.3.1. Raw Material and Installed Equipment Costs

The required amount of raw materials was estimated according to the stoichiometric amounts given in Equation (1) and Equations (11)–(14). Table 3 indicates the amount of required materials per batch with their unit price for economic evaluation for different production scales. It should be noted that both HCl and NH_4Cl streams contain water in the mixture (see its mass % in Table 3). Furthermore, the required equipment details were summarized in Table A3 in Appendix A. Moreover, Tables A4–A6 in Appendix B list the equipment unit price, annual required materials price, and utility consumption, respectively, for different production scales of the Ti powder plant. The annual materials cost can be calculated from each material unit price and the annual amount per batch by the number of batches per year in Table 2. Based on Tables A4–A6, it can be concluded that raw materials have the highest impact on production costs, regardless of the production scale. It should be noted that the SuperPro Designer software v8.5 (Scotch Plains, New Jersey, USA) has a built-in model for the calculation of equipment costs [49], based on the costs model in Peters et al. [68].

Table 3. The required amount of raw material with their unit costs for different production scale.

Raw Material	Unit Cost	Amount for Different Production Scales of Ti (kg/Batch)		
		1-t/Batch	5-t/Batch	10-t/Batch
NH ₄ Cl 3.2 M (11% NH ₄ Cl and 89% water)	0.11 \$/kg	114,106.65	570,533.24	1,141,066.48
Carbon (C)	1.00 \$/kg	1113.27	5566.37	11,132.74
Chlorine gas (Cl ₂)	1.25 \$/kg	3282.68	16,413.43	32,826.87
HCl 1 M (9.7% HCl and 90.3% water) (P-5)	0.097 \$/kg	1873.64	9368.19	18,736.37
HCl 1 M (9.7% HCl and 90.3% water) (P-8)	0.097 \$/kg	351.91	1759.52	3519.05
H ₂ gas (P-2)	8.60 \$/m ³	93.25	466.27	932.55
H ₂ gas (P-7)	8.60 \$/m ³	0.21	1.04	2.08
Ilmenite (FeTiO ₃)	4.0 \$/kg	3519.04	17,595.23	35,190.45
Magnesium hydride (MgH ₂)	143.00 \$/kg	1228.93	6144.66	12,289.32
Nitrogen gas (N ₂)	2.10 \$/m ³	323.75	1618.76	3237.52
Oxygen gas (O ₂) (from air)	0.0	529.32	2646.63	5293.26

Table 4 summarizes the purchase cost of major equipment according to the studied production scales of Ti powder, calculated using the built-in model [49]. It should be noted that the equipment capacity is directly related to the production throughput. As can be seen, the highest equipment cost was associated with the TiCl₄ reduction furnace (R-103) and MgCl₂ electrolysis cell (R-104) for the Ti production scale of 1 t/batch, and ilmenite reduction reactor (R-101) for Ti production scale of 5 t/batch and 10 t/batch.

Table 4. The total equipment cost per batch for different production scales of Ti powder in USD.

Name	1-t/Batch		5-t/Batch		10-t/Batch	
	Number	Total Costs	Number	Total Costs	Number	Total Costs
R-101	1	649,000	4	2,680,000	7	4,774,000
AFR-101	1	436,000	1	1,106,000	1	1,700,000
GR-101	1	105,000	1	174,000	1	260,000
MF-101	1	30,000	1	48,000	1	73,000
MF-102	1	30,000	1	56,000	1	85,000
R-102	1	531,000	1	661,000	1	728,000
V-101	1	29,000	1	69,000	1	101,000
R-103	1	710,000	1	844,000	1	984,000
R-104	1	712,000	1	848,000	1	989,000
R-105	1	538,000	1	671,000	1	738,000
V-102	1	60,000	1	134,000	1	229,000
Total price (\$)		3,830,000		7,291,000		10,661,000

3.3.2. Economic Analysis

Based on the economic model of Peters et al. [68], the built-in model of SuperPro Designer v8.5 (Scotch Plains, NJ, USA) [49] determines the production costs as a percentage of the capital cost and operating costs, as summarized in Table A7 in Appendix C. It is evident from Table A7 that the equipment purchase cost is the highest factor in the direct plant costs, while the construction was a significant factor in indirect plant cost. Table 5 summarizes the capital fixed costs for Ti production scales of 1, 5, and 10 t/batch. It is noteworthy that the total equipment purchase cost, process piping, installation, insulation, instrumentation, buildings, electrical, yard improvement, and auxiliary facilities are considered direct plant costs. On the other hand, engineering and construction were categorized as indirect plant costs. Other parameters such as start-up and validation, insurance, maintenance, a local tax, and the factory expenses were included in calculating the capital investment in the economic modeling by the SuperPro Designer [49]. It is evident from Table 5 that direct and indirect plant expenses increase with an increase in production scale.

Table 5. Fixed capital estimate summary for different scale of Ti powder plant in USD.

Parameter	1-t/Batch	5-t/Batch	10-t/Batch
Equipment Purchase Cost	4,697,500	9,114,000	13,326,000
Total Plant Direct Cost (TPDC)	15,539,000	29,630,000	44,344,000
Total Plant Indirect Cost (TPIC)	9,323,000	17,778,000	26,007,000
Contractor's Fee and Contingency	3,729,000	7,111,000	10,403,000
Direct Fixed Capital Cost	28,054,388	54,519,000	79,753,000

3.3.3. Unit Production Cost of Ti Metal Powder

The economic evaluation results for the investigated production scales were given in Table 6. It was considered that the Ti metal powder price is 250 USD/kg. The two main economic factors, i.e., return of investment (ROI) and internal rate of return (IRR) values, were compared for all the production scales as reported in Table 6. In general, a positive ROI value indicates that the net returns are positive since the total returns are higher than the process costs. Moreover, a project is economically feasible with a higher IRR than the minimum acceptable returns for investors [61,68]. The results in Table 6 demonstrated that maximum ROI and IRR were 39.36% and 63.20%, respectively, which was obtained for production scale of 5 t/batch. However, the ROI and IRR decreased to 35.18% and 53.83% for 10 t/batch production scale, respectively. This is mainly due to a significant increase in the total capital investment for 10 t/batch, with a marginal increase in its revenue. This leads to lower ROI and IRR as compared to the 5 t/batch production scale. Overall, the unit production cost for Ti powder ranges between 224.19 and 246.58 USD/kg Ti from this study.

Table 6. Economic performance summary for different production scale.

Parameter	1-t/Batch	5-t/Batch	10-t/Batch
Total Capital Investment (\$)	42,427,000	83,025,000	109,793,000
Operating Cost (\$/year)	138,577,000	284,499,000	286,964,000
Revenues (\$/year)	140,500,000	313,750,000	320,000,000
Net Profit (\$/year)	4,523,000	32,675,000	38,630,000
Cost Basis Annual Rate (kg MP/year) ^a	562,000	1,255,000	1,280,000
Unit Production Cost (\$/kg MP)	246.58	226.69	224.19
Unit Production Revenue (\$/kg MP)	250.00	250.00	250.00
Gross Margin (%)	1.37	9.32	10.32
Return on Investment (ROI) (%)	10.66	39.36	35.18
Payback Time (year)	9.38	2.54	2.84
Rate of Return (IRR) after taxes (%)	9.77	63.20	53.83

^a MP = Total Flow of Stream "Ti powder".

The Monte Carlo method was employed to quantify the uncertainty [69,70] for the sensitivity analysis, using Crystal Ball v11.1.2.4 add-in function in Microsoft Excel. This simulation determines which operational factors have the most significant impacts on the economic efficiency of the process. According to Table 6, the ROI (39.36%) and the unit production cost of the Ti powder (\$226.69/kg) for the Ti powder production scale of 5 t/batch were investigated for the sensitivity analysis. The distribution of model variables was summarized in Table A8 in Appendix D. In general, triangular distribution was applied for the time, and normal distribution with 10% standard deviation was used for price fluctuations. The probability distribution of ROI and Ti unit production costs are illustrated in Figure 10. It is evident from Figure 10a that the change in ROI from 10 to 70% falls within the certainty of about 76.42%. Moreover, it was observed from Figure 10b that the change in Ti unit production cost amounts from \$205 to \$250 correlated with a certainty of occurrence of about 79.37%.

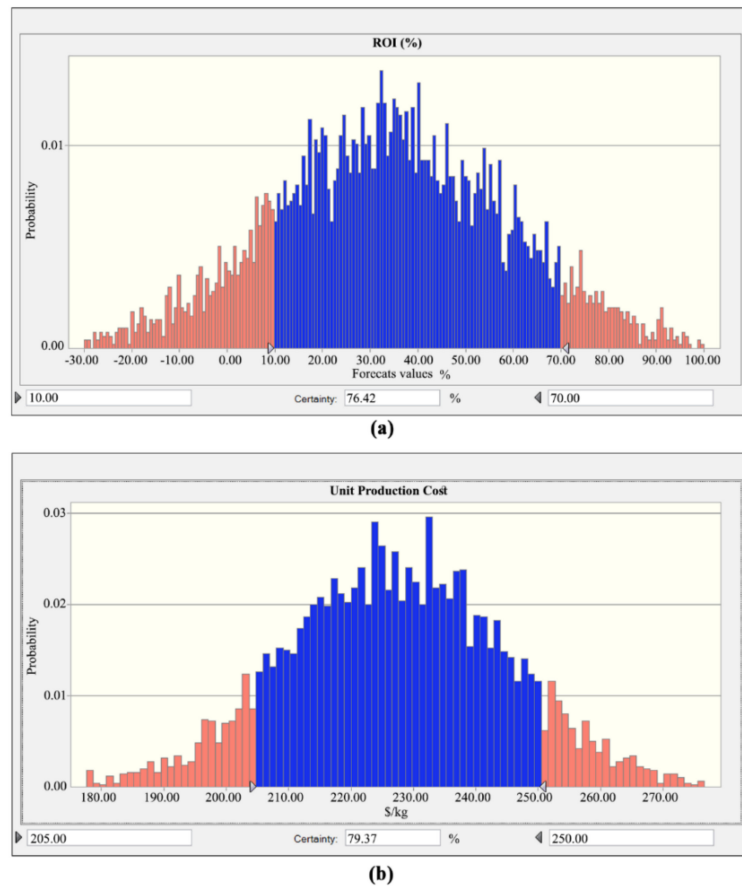


Figure 10. Probability distribution diagram after 5000 trials for (a) ROI and (b) unit production costs.

The sensitivity analysis diagrams generated by the Crystal Ball (Figure 11) reveals that the MgH_2 purchase cost was the most significant input variable on the unit production costs and ROI, which is followed by the ilmenite purchase price. Overall, the MgH_2 price has a negative impact on the economic analysis. Increasing the MgH_2 price results in lower ROI and increased unit production cost.

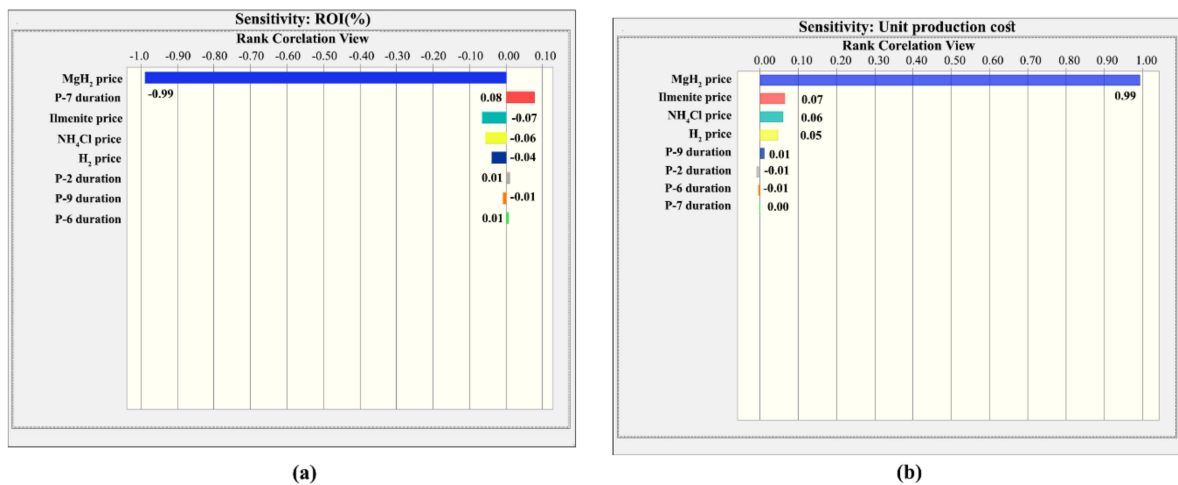


Figure 11. Contribution of uncertain parameters to the variance of (a) ROI and (b) unit production cost.

4. Conclusions

Thermodynamic assessment of TiH_2 synthesized from TiCl_4 was investigated between MgH_2 with TiCl_4 in the presence of H_2 atmosphere at a temperature range from 0 to 700 °C. The thermodynamic assessment revealed that the formation of TiH_2 was feasible in the TiCl_4 - MgH_2 reaction system. However, the molar fraction of TiCl_4 has a critical role in the reduction process. With an increase in the molar fraction of TiCl_4 above 0.4, the TiH_2 formation was impeded, and the TiCl_3 phase started to produce significantly. According to the various amounts of TiCl_4 : MgH_2 molar ratio, different products were obtained. Experimental data confirmed the thermodynamic assessment on TiH_2 formation from TiCl_4 : MgH_2 were also extracted, and findings, and it was indicated that at the reaction temperature of 500 °C for 12 h, TiH_2 powder was formed. Moreover, the TEA of Ti metal powder production was conducted for 1, 5, and 10 t/batch production scales. The modeling results indicated that the highest ROI of 39.36% with 2.54 years of payback time was achieved at 5 t/batch production scale. Moreover, sensitivity analysis showed that the MgH_2 and ilmenite purchase prices had the highest negative impact on the ROI and unit production costs. The change in the raw materials by 10% resulted in the certainty of 76.42% for ROI changing between 10% and 70%. Similarly, the certainty for the unit product cost was achieved at about 79.37% for fluctuating between 205 and 250 \$/kg. It has shown that the production of Ti powder via the TiH_2 route from ilmenite at the low-temperature range was economically feasible.

Author Contributions: Conceptualization, S.A.R.S.A.H. and D.C.Y.F.; methodology, M.R.A., S.A.R.S.A.H. and D.C.Y.F.; software, D.C.Y.F. and M.R.A.; investigation, M.R.A.; data curation, M.R.A. and D.C.Y.F.; writing—original draft preparation, M.R.A.; writing—review and editing, S.A.R.S.A.H., D.C.Y.F., and A.R.M.; project administration, S.A.R.S.A.H. and A.R.M.; funding acquisition, S.A.R.S.A.H. All authors have read and agreed to the published version of the manuscript.

Funding: This research was funded by the following grants: Ministry of Higher Education Malaysia for Prototype Research Grant Scheme with Project Code: PRGS/2/2019/TK05/USM/02/1, MOHE Fundamental Research Grant Scheme (FRGS) grant no: 203/PBAHAN/6071364, and USM Research University Individual (RUI) grant no: 1001/PBAHAN/814273. Further support by USM research grant was entitled Geran Bridging # 304/PBAHAN/6316116 and Nippon Sheet Glass Research Grant (NSGRG) (No. 304/PBAHAN/650360/N120).

Acknowledgments: The authors wish to thank Universiti Sains Malaysia (USM) and Ministry of Higher Education (MOHE) of Malaysia for supporting this work.

Conflicts of Interest: The authors declare no conflict of interest.

Appendix A. Process Simulation Setting

Table A1. Scheduling summary for the simulation model of 1000 kg Ti/batch.

Procedure	Operation	Process Time ^a (h)	Start Time (h)	End Time (h)
P-1	Grinding ilmenite below 75 μm	1.25	0	1.25
P-1/2	Mixing ilmenite with coal	1.25	1.25	2.50
P-2	Ilmenite reduction with H_2 - N_2 gases mixture at 1250 °C	12.31	2.50	14.81
P-3	TiN with Fe aeration leaching at 90 °C to remove Fe particles	9.00	14.81	23.81
P-4	Filtration to separate TiN from Fe particles	4.25	23.81	28.06
P-4/1	Filtration to separate Fe_2O_3 from NH_4Cl solution	4.25	23.81	28.06
P-5	Acid washing at room temperature to remove any excess Fe particles from TiN	7.43	28.06	35.49
P-5/1	FeCl_2 Storage for sewage treatment industries	7.32	32.85	40.17
P-6	TiN chlorination process at 350 °C	7.64	32.85	40.49
P-7	TiCl_4 Reduction process in H_2 atmosphere at 500 °C	14.00	40.49	54.49
P-8	Water washing at room temperature to remove impurities from TiH_2	1.25	54.49	55.74
P-8/1	MgCl_2 electrolysis to produce Mg metal	3.50	55.74	59.24
P-9	TiH_2 dehydrogenation to Ti powder at 700 °C	4.50	55.74	60.24
P-10	H_2 gas Storage	3.50	56.24	59.24

^a Processing time included the required time for charging and transferring out the materials.

Table A2. Specifications of simulation model.

Process	Description
Reduction reactor at P-2	heating for 3 h at 1250 °C, extent of reaction 100%
Aeration leaching at P-3	leaching at 90 °C for 7 h, extent of leaching 95%
Microfiltration at P-4	filtration for 2 h with recovery yield of 90%
Microfiltration at P-4/1	filtration for 4 h with recovery yield of 90%
Acid washing in P-5	washing for 30 min and separation for 1 h with 100% recovery at room temperature
Chlorination reaction at P-6	heating for 5 h at 350 °C, extent of chlorination 95%
Reduction reaction in P-7	heating for 12 h at 500 °C, extent of reaction 95%
Acid washing and separation in P-8	washing for 1 h with 100% recovery after filtration
Electrolysis in P-8/1	reaction duration for 1 h at room temperature, extent of separation 100%
Dehydrogenation in P-9	heating for 3 h at 700 °C, extent of reaction 100%

Table A3. Equipment types and size for Ti powder plant for different production scale of Ti powder.

Name	Type	Production Scale		
		1-t/Batch	5-t/Batch	10-t/Batch
R-101	Stirred Reactor	1.21 m ³	1.52 m ³	1.73 m ³
AFR-101	Air-Lift Fermentor	124,952.11 L	624,760.53 L	1,249,521.06 L
GR-101	Grinder	3519.05 kg/h	17,595.23 kg/h	35,190.46 kg/h
MF-101	Microfilter	2.15 m ²	10.74 m ²	21.48 m ²
MF-102	Microfilter	2.80 m ²	14.00 m ²	28.01 m ²
SFR-101	Shake FlaskRack	2224.00 L	11,120.00 L	22,240.00 L
MX-101	Mixer	4632.32 kg/h	23,161.60 kg/h	46,323.21 kg/h
R-102	Stirred Reactor	277.62 L	1388.08 L	2776.15 L
V-101	Horizontal Tank	1946.24 L	9731.18 L	19,462.35 L
R-103	Stirred Reactor	2312.99 L	11,564.93 L	23,129.86 L
WSH-101	SWasher (Bulk Flow)	5149.38 kg/h	12,873.45 kg/h	12,873.45 kg/h
R-104	Stirred Reactor	2361.94 L	11,809.69 L	23,619.38 L
R-105	Stirred Reactor	308.76 L	1543.78 L	3087.57 L
V-102	Horizontal Tank	3214.24 L	16,071.20 L	32,142.41 L

Appendix B. Process Costs

Table A4. Equipment unit cost and required number for different production scale of Ti powder.

Name	1-t/Batch		5-t/Batch		10-t/Batch	
	Unit Cost (\$)	Number	Unit Cost (\$)	Number	Unit Cost (\$)	Number
R-101	649,000	1	670,000	4	682,000	7
AFR-101	436,000	1	1,106,000	1	1,700,000	1
GR-101	105,000	1	174,000	1	260,000	1
MF-101	30,000	1	48,000	1	73,000	1
MF-102	30,000	1	56,000	1	85,000	1
SFR-101	0	1	0	1	0	1
MX-101	0	1	0	1	0	1
R-102	531,000	1	661,000	1	728,000	1
V-101	29,000	1	69,000	1	101,000	1
R-103	710,000	1	844,000	1	984,000	1
WSH-101	0	1	0	2	0	4
R-104	712,000	1	848,000	1	989,000	1
R-105	538,000	1	671,000	1	738,000	1
V-102	60,000	1	134,000	1	229,000	1

Table A5. Annual materials cost for different production scale of Ti powder.

Material	1 t/Batch	5 t/Batch	10 t/Batch
Hydrogen (m ³)	5,103,992	11,397,705	11,624,751
Nitrogen (m ³)	309,694	691,576	705,352
Ammonium chloride (kg)	7,054,073	15,752,423	16,066,216
Water (kg)	0	0	0
Oxygen (kg)	0	0	0
Ilmenite (kg)	7,910,815	17,665,611	18,017,515
Hydrochloric acid (kg)	121,323	270,926	276,323
Carbon (kg)	625,660	1,397,160	1,424,992
Chlorine (kg)	2,306,088	5,149,716	5,252,300
Magnesium hydride (kg)	98,764,347	220,550,276	224,943,708
Total price (\$)	122,195,993	272,875,393	278,311,158

NOTE: Bulk material consumption amount includes material used such as: raw material, cleaning agent, and heat transfer agent (if utilities are included in the operating cost).

Table A6. Annual utilities cost for different production scale of Ti powder.

Parameter	Unit Cost (\$)	1 t/Batch		5 t/Batch		10 t/Batch	
		Amount	Cost (\$)	Amount	Cost (\$)	Amount	Cost (\$)
Std Power (Kwh)	0.100	249,994	24,999	558,261	55,826	569,382	56,938
Steam (MT)	4.200	7154	30,045	15,975	67,094	16,293	68,431
Chilled Water (MT)	0.400	4138	1655	9241	3696	9425	3770
Steam (High P) (MT)	20.000	10	197	22	441	22	450
TOTAL (\$)		56,897		127,057		129,588	

Appendix C. Percentage Coefficient for Capital Cost

Table A7. The percentage coefficient of direct plant cost factors.

Name	Percentage	Name	Percentage
Piping	35% EPC ¹	Auxiliary facilities	40% EPC
Instrumentation	40% EPC	Engineering fee	25% DC ²
Insulation	3% EPC	Construction	35% DC
Electrical facilities	10% EPC	Contractor fee	5% (DC + IC ³)
Building	45% EPC	Contingency fee	10% (DC + IC)
Yard improvement	15% EPC		

¹ Equipment purchase cost, ² direct plant cost, and ³ indirect plant cost.

Appendix D. Sensitivity Analysis Assumptions

Table A8. Input parameters used for sensitivity analysis.

Variable	Base Case Values	Distribution	Variation and Range
Reduction process in P-7	14	Triangular	12.60–15.40
Dehydrogenation process in P-9	4.5	Triangular	4.05–4.95
R-102 stirred reactor cost	661,000	Normal	S.D. = 0.1
R-103 stirred reactor cost	844,000	Normal	S.D. = 0.1
R-104 stirred reactor cost	848,000	Normal	S.D. = 0.1
Hydrogen price	11,397,705	Normal	S.D. = 0.1
Ammonium chloride price	15,752,423	Normal	S.D. = 0.1
Ilmenite price	17,665,611	Normal	S.D. = 0.1
MgH ₂ price	220,550,276	Normal	S.D. = 0.1
Chlorine price	5,149,716	Normal	S.D. = 0.1

S.D.: Standard deviation.

References

1. Ezugwu, E.; Bonney, J.; Yamane, Y. An overview of the machinability of aeroengine alloys. *J. Mater. Process. Technol.* **2003**, *134*, 233–253. [\[CrossRef\]](#)
2. Boyer, R.R. Attributes, characteristics, and applications of titanium and its alloys. *JOM* **2010**, *62*, 21–24. [\[CrossRef\]](#)
3. Crowley, G. How to Extract Low-Cost Titanium. *Adv. Mater. Process* **2003**, *161*, 25–27.
4. Fray, D.J. Novel methods for the production of titanium. *Int. Mater. Rev.* **2008**, *53*, 317–325. [\[CrossRef\]](#)
5. Takeda, O.; Uda, T.; Okabe, T.H. Rare Earth, Titanium Group Metals, and Reactive Metals Production. In *Treatise on Process Metallurgy, Volume 3: Industrial Processes, Part A*; Seetharaman, S., Mclean, A., Guthrie, R., Sridhar, S., Eds.; Elsevier: Oxford, UK, 2014; pp. 995–1069.
6. Van Vuuren, D.S. A Critical Evaluation of Processes to Produce Primary Titanium. *J. S. Afr. Inst. Min. Metall.* **2009**, *109*, 455–461.
7. Kraft, E.H. *Summary of Emerging Titanium Cost Reduction Technologies*; Study for US DoE and ORNL/Subcontract 4000023694; EHK Technology: Vancouver, WA, USA, 2004.
8. McCracken, C.G.; Motchenbacher, C.; Barbis, D.P. Review of titanium-powder-production methods. *Int. J. Powder Metall.* **2010**, *46*, 19–26.
9. Van Vuuren, D.S.; Oosthuizen, S.J.; Heydenrych, M.D. Titanium production via metallothermic reduction of $TiCl_4$ in molten salt: Problems and products. *J. S. Afr. Inst. Min. Metall.* **2011**, *111*, 141–148.
10. Doblin, C.; Chryst, A.; Monch, A. Titanium Powder from the TiRO™ Process. *Key Eng. Mater.* **2012**, *520*, 95–100. [\[CrossRef\]](#)
11. Oosthuizen, S.J. In search of low cost titanium: The Fray Farthing Chen (FFC) Cambridge process. *J. S. Afr. Inst. Min. Metall.* **2011**, *111*, 199–202.
12. Chen, W.; Yamamoto, Y.; Peter, W.; Clark, M.; Nunn, S.; Kiggans, J.; Muth, T.; Blue, C.; Williams, J.; Akhtar, K. The investigation of die-pressing and sintering behavior of ITP CP-Ti and Ti-6Al-4V powders. *J. Alloy. Compd.* **2012**, *541*, 440–447. [\[CrossRef\]](#)
13. Van Vuuren, D.S. Direct titanium powder production by metallothermic processes. In *Titanium Powder Metallurgy: Science, Technology and Applications*; Qian, M., Froes, F.H., Eds.; Elsevier: Amsterdam, The Netherlands, 2015; pp. 69–93.
14. Fang, Z.Z.; Middlemas, S.; Guo, J.; Fan, P. A New, Energy-Efficient Chemical Pathway for Extracting Ti Metal from Ti Minerals. *J. Am. Chem. Soc.* **2013**, *135*, 18248–18251. [\[CrossRef\]](#)
15. Zhang, Y.; Fang, Z.Z.; Xia, Y.; Sun, P.; Devener, B.V.; Free, M.; Lefler, H.; Zheng, S. Hydrogen assisted magnesiothermic reduction of TiO_2 . *Chem. Eng. J.* **2017**, *308*, 299–310. [\[CrossRef\]](#)
16. Ahmadi, E.; Yashima, Y.; Suzuki, R.O.; Rezan, S. Formation of Titanium Sulfide from Titanium Oxycarbonitride by CS_2 Gas. *Metall. Mater. Trans. B* **2018**, *49*, 1808–1821. [\[CrossRef\]](#)
17. Suzuki, R.O.; Ono, K.; Teranuma, K. Calciothermic reduction of titanium oxide and in-situ electrolysis in molten $CaCl_2$. *Metall. Mater. Trans. B* **2003**, *34*, 287–295. [\[CrossRef\]](#)
18. Suzuki, R.O.; Natsui, S.; Kikuchi, T. Recent Studies on Titanium Refining: 2017–2020. *Mater. Trans.* **2021**, *62*, 905–913. [\[CrossRef\]](#)
19. U.S. Geological Survey, Mineral Commodity Summaries, February 2019. Titanium Statistics and Information. Available online: <https://prd-wret.s3-us-west-2.amazonaws.com/assets/palladium/production/atoms/files/mcs-2019-timin.pdf> (accessed on 29 June 2021).
20. Geetha, K.; Surender, G. Experimental and modelling studies on the aeration leaching process for metallic iron removal in the manufacture of synthetic rutile. *Hydrometallurgy* **2000**, *56*, 41–62. [\[CrossRef\]](#)
21. Yaraghi, A.; Sapri, M.H.A.; Baharun, N.; Rezan, S.A.; Shoparwe, N.I.; Ramakrishnan, S.; Ariffin, K.S.; Fauzi, M.A.; Zabidi, H.B.; Ismail, H.; et al. Aeration Leaching of Iron from Nitrided Malaysian Ilmenite Reduced by Polystyrene-Coal Reductant. *Procedia Chem.* **2016**, *19*, 715–720. [\[CrossRef\]](#)
22. Ahmadi, E.; Rezan, S.A.; Baharun, N.; Ramakrishnan, S.; Fauzi, M.N.A.; Zhang, G. Chlorination Kinetics of Titanium Nitride for Production of Titanium Tetrachloride from Nitrided Ilmenite. *Metall. Mater. Trans. B* **2017**, *48*, 2354–2366. [\[CrossRef\]](#)
23. Ahmadi, E.; Fauzi, M.N.A.; Hussin, H.; Baharun, N.; Ariffin, K.S.; Rezan, S.A. Synthesis of titanium oxycarbonitride by carbothermal reduction and nitridation of ilmenite with recycling of polyethylene terephthalate (PET). *Int. J. Min. Met. Mater.* **2017**, *24*, 444–454. [\[CrossRef\]](#)
24. Ardani, M.R.; Al Janabi, A.S.M.; Udayakumar, S.; Rezan, S.A.; Mohamed, A.R.; Lee, H.L.; Ibrahim, I. Reduction of $TiCl_4$ to TiH_2 with CaH_2 in presence of Ni powder. In *Rare Metal Technology 2019*; Azimi, G., Kim, H., Alam, S., Ouchi, T., Neelameggham, N.R., Baba, A.A., Eds.; Springer: Cham, Switzerland, 2019; pp. 131–144.
25. Ardani, M.R.; Fauzi, M.N.A.; Rezan, S.A.; Mohamed, A.R.; Lee, H.L.; Ibrahim, I. Thermodynamic Investigation of Titanium Hydride Formation from Reduction of Titanium (IV) Chloride with Magnesium Hydride in Presence of Hydrogen Atmosphere. *MATEC Web Conf.* **2020**, *321*, 07014. [\[CrossRef\]](#)
26. Ardani, M.R.; Rezan, S.A.; Lee, H.L.; Mohamed, A.R.; Ibrahim, I. Low Temperature Synthesis Method of TiH_2 Powder from $TiCl_4$ Reduction with MgH_2 . In *Proceedings of the TMS 2020 149th Annual Meeting & Exhibition Supplemental Proceedings*, San Diego, CA, USA, 23–27 February 2020; The Minerals, Metals & Materials Society, Ed.; Springer: Cham, Switzerland, 2020; pp. 1669–1679.
27. Robertson, M.I.; Schaffer, G.B. Comparison of sintering of titanium and titanium hydride powders. *Powder Metall.* **2010**, *53*, 12–19. [\[CrossRef\]](#)
28. Fang, Z.Z.; Fan, P.; Middlemas, S.; Guo, J.; Zhang, Y.; Free, M.; Sathyapalan, A.; Xia, Y. Producing a Titanium Product. U.S. Patent US2016/0194733 A1, 7 July 2016.

29. Granjo, J.F.O.; Oliveira, N.M.C. Process Simulation and Techno-Economic Analysis of the Production of Sodium Methoxide. *Ind. Eng. Chem. Res.* **2016**, *55*, 156–167. [CrossRef]
30. Rodrigues, V.H.; de Melo, M.M.; Portugal, I.; Silva, C.M. Simulation and techno-economic optimization of the supercritical CO₂ extraction of Eucalyptus globulus bark at industrial scale. *J. Supercrit. Fluids* **2019**, *145*, 169–180. [CrossRef]
31. Larbi, F.; García, A.; del Valle, L.J.; Hamou, A.; Puiggali, J.; Belgacem, N.; Bras, J. Simulation basis for a techno-economic evaluation of chitin nanomaterials production process using Aspen Plus[®] software. *Data Brief* **2018**, *20*, 1556–1560. [CrossRef] [PubMed]
32. Alfonso-Cardero, A.; Pagés-Díaz, J.; Contino, F.; Rajendran, K.; Lorenzo-Llanes, J. Process simulation and techno-economic assessment of vinasse-to-biogas in Cuba: Deterministic and uncertainty analysis. *Chem. Eng. Res. Des.* **2021**, *169*, 33–45. [CrossRef]
33. Petrides, D.; Sapidou, E.; Calandranis, J. Computer-aided process analysis and economic evaluation for biosynthetic human insulin production—A case study. *Biotechnol. Bioeng.* **1995**, *48*, 529–541. [CrossRef] [PubMed]
34. Tan, J.; Foo, D.C.Y.; Kumaresan, S.; Aziz, R.A. Debottlenecking of a Batch Pharmaceutical Cream Production. *Pharm. Eng.* **2006**, *26*, 72–84.
35. Koulouris, A.; Calandranis, J.; Petrides, D.P. Throughput Analysis and Debottlenecking of Integrated Batch Chemical Processes. *Comput. Chem. Eng.* **2000**, *24*, 1387–1394. [CrossRef]
36. Athimulam, A.; Kumaresan, S.; Foo, D.; Sarmidi, M.; Aziz, R. Modelling and Optimization of Eurycoma longifolia Water Extract Production. *Food Bioprod. Process.* **2006**, *84*, 139–149. [CrossRef]
37. Alshekhlhi, O.; Foo, D.C.Y.; Hii, C.L.; Law, C.L. Process Simulation and Debottlenecking for An Industrial Cocoa Manufacturing Process. *Food Bioprod. Process.* **2011**, *89*, 528–536. [CrossRef]
38. Noor, N.Z.M.; Foo, D.C.Y.; Rahman, B.A.; Aziz, R.A. Modelling and Uncertainty Analysis for Pilot Scale Monoclonal Antibody Production. *Pharm. Eng.* **2014**, *34*, 40–54.
39. Gebremariam, S.N.; Marchetti, J.M. Process simulation and techno-economic performance evaluation of alternative technologies for biodiesel production from low value non-edible oil. *Biomass Bioenergy* **2021**, *149*, 106102. [CrossRef]
40. Lim, S.S.; Foo, D.C. Simulation and scale-up study for a chitosan–TiO₂ nanotubes scaffold production. *Food Bioprod. Process.* **2017**, *106*, 108–116. [CrossRef]
41. Sayar, N.A.; Şam, S.D.; Pinar, O.; Serper, D.; Akbulut, B.S.; Kazan, D.; Sayar, A.A. Techno-economic analysis of caffeine and catechins production from black tea waste. *Food Bioprod. Process.* **2019**, *118*, 1–12. [CrossRef]
42. Pang, Y.X.; Yan, Y.; Foo, D.C.; Sharmin, N.; Zhao, H.; Lester, E.; Wu, T.; Pang, C.H. The influence of lignocellulose on biomass pyrolysis product distribution and economics via steady state process simulation. *J. Anal. Appl. Pyrolysis* **2020**, *158*, 104968. [CrossRef]
43. Udayakumar, S.; Baharun, N.; Rezan, S.A.; Ismail, A.F.; Takip, K.M. Economic evaluation of thorium oxide production from monazite using alkaline fusion method. *Nucl. Eng. Technol.* **2021**, *53*, 2418–2425. [CrossRef]
44. Ardani, M.R.; Sheikh Abdul Hamid, S.A.R.; Lee, H.L.; Mohamed, A.R.; Ibrahim, I. Characterization of TiH₂ Powders Produced from TiCl₄-MgH₂ Reactions under Hydrogen Atmosphere. *J. Mater. Eng. Perform.* **2021**, *30*, 3243–3257. [CrossRef]
45. Ardani, M.R.; Sheikh Abdul Hamid, S.A.R.; Mohamed, A.R. Synthesis of TiH₂ powder from ilmenite using MgH₂ under H₂ atmosphere. *Mater. Lett.* **2021**, *298*, 129997. [CrossRef]
46. Ahmadi, E.; Shoparwe, N.I.; Ibrahim, N.; Sheikh Abdul Hamid, S.A.R.; Baharun, N.; Ariffin, K.S.; Hussin, H.; Fauzi, M.N.A. The Effects of Experimental Variables on Iron Removal from Nitrided Malaysian Ilmenite by Becher Process. In *Extraction 2018*; Davis, B., Moats, M.S., Wang, S., Gregurek, D., Kapusta, J., Battle, T.P., Schlesinger, M.E., Flores, G.R.A., Jak, E., Goodall, G., et al., Eds.; The Minerals, Metals & Materials Series; Springer: Cham, Switzerland, 2018; pp. 1383–1396.
47. Yaraghi, A.; Sapri, M.H.A.; Ahmadi, E.; Baharun, N.; Rezan, S.; Shoparwe, N.F.; Ramakrishnan, S.; Ariffin, K.S.; Fauzi, M.N.A.; Zabidi, H.; et al. Microstructural Study of Leached Nitrided Malaysian Ilmenite with Coal-Polystyrene Reductant. *Key Eng. Mater.* **2016**, *701*, 132–137. [CrossRef]
48. Roine, A. *Outokumpu HSC Chemistry, Chemical Reaction and Equilibrium Software with Extensive Thermochemical Database*; Finland Outokumpu Research Oy: Temper, Finland, 2006.
49. Intelligen. *SuperPro Designer User's Guide*; Intelligen, Inc.: Scotch Plains, NJ, USA, 2006.
50. Stull, D.R.; Prophet, H. *JANAF Thermochemical Tables*, 2nd ed.; National Standard Reference Data System: USA, 1971. Available online: <https://www.govinfo.gov/app/details/GOVPUB-C13-bfd606acc2525ccef2762b19002a6d4f> (accessed on 30 August 2021).
51. Barin, I. *Thermochemical Data of Pure Substances*, 3rd ed.; Wiley-VCH: Weinheim, Germany, 1995.
52. Rezan, S.; Zhang, G.; Ostrovski, O. Carbothermal Reduction and Nitridation of Titanium Dioxide in a H₂-N₂ Gas Mixture. *J. Am. Ceram. Soc.* **2011**, *94*, 3804–3811. [CrossRef]
53. Hui, Y.J.; Shoparwe, N.I.; Rezan, S.A.; Baharun, N.; Sreekantan, S.; Fauzi, A.M.N. Effect of Carbon Reductant on the Formation of Copper Doped Titanium Oxycarbonitride by Carbothermal Reduction and Nitridation. In *8th International Symposium on High-Temperature Metallurgical Processing*; Hwang, J.Y., Jiang, T., Kennedy, M.W., Yucel, O., Pistorius, P., Seshadri, V., Zhao, B., Gregurek, D., Keskinikilic, E., Eds.; The Minerals Metals & Materials Series; Springer: Cham, Switzerland, 2017.
54. Udayakumar, S.; Sadaqi, A.; Ibrahim, N.; Fauzi, M.N.A.; Ramakrishnan, S.; Rezan, S.A. Mathematical Modelling of Titanium Hydride Formation from Titanium Tetrachloride with Magnesium Hydride using Matlab. *J. Phys. Conf. Ser.* **2018**, *1082*, 012037–012043. [CrossRef]

55. Udayakumar, S.; Sadaqi, A.; Ibrahim, N.; Fauzi, M.N.A.; Ramakrishnan, S.; Rezan, S.A. Formation of Titanium Hydride from the Reaction Between Magnesium Hydride and Titanium Tetrachloride. *J. Phys. Conf. Ser.* **2018**, *1082*, 012003. [[CrossRef](#)]
56. Lewis, R.J. *Hawley's Condensed Chemical Dictionary*, 15th ed.; John Wiley & Sons, Inc.: Hoboken, NJ, USA, 2007.
57. Rezan, S.; Zhang, G.; Ostrovski, O. Carbothermal Reduction and Nitridation of Ilmenite Concentrates. *ISIJ Int.* **2012**, *52*, 363–368. [[CrossRef](#)]
58. Rezan, S.A.; Zhang, G.Q.; Ostrovski, O. Phase Development in Carbothermal Reduction and Nitridation of Ilmenite Concentrates. *High Temp. Mater. Process.* **2012**, *31*, 381–388. [[CrossRef](#)]
59. Teyssandier, F.; Allendorf, M.D. Thermodynamics and Kinetics of Gas-Phase Reactions in the Ti-Cl-H System. *J. Electrochem. Soc.* **1998**, *145*, 2167–2178. [[CrossRef](#)]
60. Zhang, Y.; Wang, C.; Liu, Y.; Liu, S.; Xiao, S.; Chen, Y. Surface Characterizations of TiH₂ Powders before and after Dehydrogenation. *Appl. Surf. Sci.* **2017**, *410*, 177–185. [[CrossRef](#)]
61. Couper, J.R.; Herts, D.W.; Smith, L. Process Economics. In *Perry's Chemical Engineers' Handbook*, 8th ed.; Green, D., Perry, R., Eds.; McGraw-Hill: New York, NY, USA, 2007; pp. 9/1–9/56.
62. Sanjith, U.; Choong, W.; Sivakumar, R.; Fauzi, M.; Rezan, S. Kinetic modelling of oxidation of metallic iron to iron sulfate from iron-titanium oxycarbonitride composite. *Mater. Today Proc.* **2019**, *17*, 525–533. [[CrossRef](#)]
63. Becher, R.G.; Canning, R.G.; Goodheart, B.A.; Uusna, S. A new process for upgrading ilmenite mineral sands. *Proc. Aust. Min. Metall.* **1965**, *214*, 21–44.
64. Liu, J.; He, K.; Tang, S.; Wang, T.; Zhang, Z. A comparative study of ferrous, ferric and ferrate pretreatment for ceramic membrane fouling alleviation in reclaimed water treatment. *Sep. Purif. Technol.* **2019**, *217*, 118–127. [[CrossRef](#)]
65. Swaminathan, K.; Subramanian, C.; Rao, C.S. The pressure oxidation of acidic FeCl₂ solution with oxygen. *Hydrometallurgy* **1981**, *6*, 339–346. [[CrossRef](#)]
66. Ahmadi, E.; Sheikh Abdul Hamid, S.A.R.; Hussin, H.; Baharun, N.; Ramakrishnan, S.; Ariffin, K.S.; Fauzi, A.M.N. The Preparation of Iron-Free TiCl₄ from Reduced and Nitrided Ilmenite by Polyethylene Terephthalate. *INROADS* **2016**, *5*, 11–16.
67. Moxson, V.S.; Duz, V.A.; Klevtsov, A.G.; Sukhoplyuev, V.D.; Sopka, M.D.; Shuvalov, Y.V.; Matviychuk, M. Manufacturing Pure Titanium Hydride Powder and Alloyed Titanium Hydride Powders by Combined Hydrogen-Magnesium Reduction of Metal Halides. U.S. Patent 9067264, 30 June 2015.
68. Peters, M.S.; Timmerhaus, K.D.; West, R.E. *Plant Design and Economics for Chemical Engineers*, 5th ed.; McGraw-Hill: New York, NY, USA, 2003.
69. Achilleos, E.C.; Calandranis, J.C.; Petrides, D.P. Quantifying the impact of uncertainty parameters in the batch manufacturing of active pharmaceutical ingredients. *Pharm. Eng.* **2006**, *26*, 1–6.
70. Heinzle, E.; Biwer, A.P.; Cooney, C.L. *Development of Sustainable Bioprocesses: Modelling and Assessment*; Wiley: Hoboken, NJ, USA, 2007.